Journal of Geochemical Exploration 157 (2015) 66–76

Contents lists available at ScienceDirect

Journal of Geochemical Exploration

journal homepage: www.elsevier.com/locate/jgeoexp

Mineralogy and geochemistry of a clogged mining reservoir affected by historical acid mine drainage in an abandoned mining area

T. Valente [a,b,*], J.A. Grande [b], M.L. de la Torre [b], P. Gomes [a,b], M. Santisteban [b], J. Borrego [b], M.A. Sequeira Braga [a]

[a] Instituto de Ciências da Terra (ICT), DCT (ECUM) Polo da Universidade do Minho, Universidade do Minho, Campus de Gualtar, 4710-057 Braga, Portugal
[b] Centro de Investigación para la Ingeniería en Minería Sostenible, Escuela Técnica Superior de Ingeniería, Universidad de Huelva, Ctra. Palos de la Frontera, s/n, 21819 Palos de la Frontera, Huelva, Spain

ARTICLE INFO

Article history:
Received 14 October 2014
Revised 19 May 2015
Accepted 31 May 2015
Available online 3 June 2015

Keywords:
Acid mine drainage
Clogged reservoir
Clay minerals
Jarosite
Metal(oids)
Riotinto
SW Spain

ABSTRACT

The present study is focused on a water reservoir that is under the influence of AMD in the historic mining area of Riotinto (SW Spain). Transport of particulate matter and chemical precipitation within the reservoir has caused its clogging. Hydrochemical, geochemical and mineralogical characterization allowed to assess the degree of contamination by trace elements.

The results indicate high average concentrations of metals and metalloids in water and sediments. The sediments are strongly enriched in As, Pb, Cu, and Zn, which occur with concentrations >1000 mg/kg. Highest accumulation was observed for As and Pb, which gave enrichment factors in the range 358–471, indicative of extreme pollution. Geochemical trends show strong correlation between major elements, including Fe and Al, mobilized from the source material.

Mineralogy of the clogging material showed a short-range of spatial variability. Among the newly formed phases jarosite and goethite are the most abundant. They are especially concentrated in the clay size fraction. Combining results about chemistry of the sediments and mineral distribution suggests that As is being retained by both clay and iron-rich minerals. Furthermore, results indicate that jarosite forms directly from sulphide oxidation, whereas goethite may result from transformations undergone in the reservoir.

1. Introduction

One of the most serious problems of environmental contamination is the formation of acid mine drainage, globally known by the acronym AMD. The severity of the problem lies in its intensity and magnitude, associated with a generally irreversible character (Carro et al., 2011; Grande et al., 2013a). This process results from sulphide oxidation, in particular iron sulphides such as pyrite (FeS_2). The reactions occur when sulphide minerals are exposed to weathering, generating acidity and sulphates, together with the mobilization of trace elements. Detailed information about the complex chain of biotic and abiotic reactions that involve the oxidative dissolution of pyrite can be found in the classical references of McKibben and Barnes (1986), Evangelou and Zhang (1995), Nordstrom and Southam (1997), Nordstrom and Alpers (1999), and Keith and Vaughan (2000).

As a consequence of the global process, the affected water systems may present pH values less than 2.5 and very high concentrations of sulphate and metals, which lead to strong degradation of the environment (*e.g.*, Grande, 2011; Gray, 1996).

AMD is a global problem, with severe consequences in metallogenetic provinces with sulphides around the world. It represents a dangerous type of contamination with consequences for health, especially if it reaches water reservoirs. The presence of high contents of metals and arsenic is a typical problem that can be found in many abandoned mining areas world widely (Borba and Figueiredo, 2003; Cheng et al., 2009; Iskandar et al., 2012).

In the SW of Europe, major problems occur in the Iberian Pyrite Belt (IPB) (Fig. 1), which is known worldwide by the intensity of the AMD processes, related with the exploitation of sulphides (Carro et al., 2011; Elbaz-Poulichet et al., 2001; Grande et al., 2013a; Sánchez-España et al., 2005). The climate conditions together with the geology and mining history have promoted a scenario where numerous water reservoirs have signs of contamination by AMD (Grande et al., 2013b). The present study was performed in one of these sites — the Marismillas reservoir, located in the Riotinto area (Fig. 1). It receives water from the Tinto River, known by its historical high levels of contamination by AMD. This river basin has been focus of much attention, with numerous studies dedicated to its hydrochemistry (*e.g.*, Cánovas et al., 2008; de la Torre et al., 2009; Grande et al., 2011; Nieto et al., 2013; Sánchez-Rodas et al., 2005; Sarmiento et al., 2009; Sobron et al., 2007; Vicente-Martorell et al., 2009), to sediment geochemistry, with works such as those by Galán et al. (2003), Ruiz et al. (2008), and Cáceres et al. (2013) as well

* Corresponding author.
E-mail address: teresav@dct.uminho.pt (T. Valente).

http://dx.doi.org/10.1016/j.gexplo.2015.05.016
0375-6742/

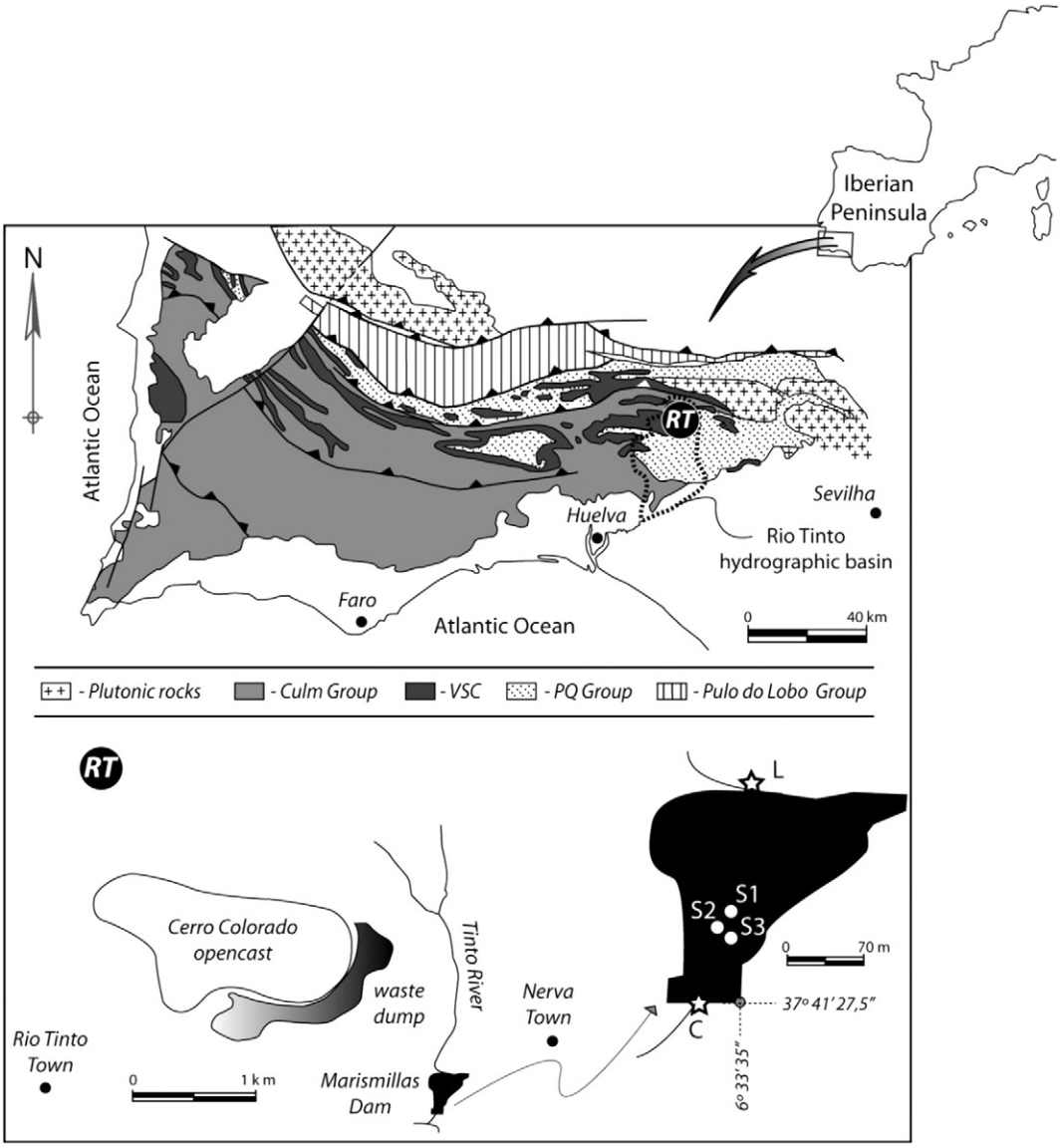

Fig. 1. Location of study site with identification of water samples (L and C) and sediment samples (S1, S2, and S3). Geological map adapted from Tornos (2006).

as soils (Fernández-Caliani et al., 2009). Also, due to its severe acidic contamination, microbe interactions and extreme ecology have been topics of research, as in the works of Fernández-Remolar et al. (2004), López-Archilla et al. (2004), Amils et al. (2007) and Stoker et al. (2008) among others.

The Marismillas reservoir has been receiving soluble contaminants as well as particulate matter for decades. Consequently, today, the reservoir is clogged by the accumulation of materials related with the evolution of AMD originated in the Riotinto complex.

Although there is an extensive bibliography on the subjects of Tinto River and Riotinto Mine, geochemical and mineralogical evolution undergone by water reservoirs submitted to extreme AMD and suffering clogging process remains a relevant topic of research. Therefore, the following specific objectives were defined for the present study: i) to describe the hydrochemistry of the acidic solution; ii) to understand the geochemical and mineralogical behaviour of the material that has been successively accumulated in the dam; and iii) to assess the relationship between the enrichment processes and the presence of secondary mineral phases. This integrated approach allows understanding the enrichment processes that may have environmental and even economic relevance in the IBP and other historical mining regions.

2. Site description

2.1. Geology and historic mining

The Marismillas reservoir is located just inside the Riotinto complex (RT), in the Iberian Pyrite Belt, SW Spain (Fig. 1). Here, metal mining has a long tradition, defining a world-class volcanogenic massive sulphide province, with more than 5000 years of mining history (Davis et al., 2000). Nowadays, several mining fields reopen and the economic interest lies on the base metals as well as precious and strategic metals as demonstrated by the intensive exploration activities (Adamides, 2013; Carvalho et al., 2011; De Oliveira et al., in press).

In the Riotinto mining district, the water and sediments will be strongly controlled by the geology of the ore deposits and host rocks. The local stratigraphic sequence comprises: i) slates and quartzites of the PQ group, ii) slates with interbedded basalt flows and volcanoclastic mafic rocks, iii) massive felsic rocks also interbedded with slate; and

iv) dark slates with conglomerates, purple and green slates and massive sulphides covered by a chert level. Regarding mineralization, it is possible to find three types, though they differ in intensity: sulphide stockwork in the volcanic rocks and slates, stratiform massive sulphides, and gossan formed by supergenic weathering (Tornos, 2006). The stockwork mineralization has a mineral paragenesis comprising: pyrite + chalcopyrite + galena + sphalerite + magnetite + quartz + chlorite + calcite + barite + sericite. Regarding stratiform sulphides, they form monotonous accumulations, mainly of pyrite with minus chalcopyrite, galena, tetrahedrite, stannite, and bornite. On the topic of host rock alteration, mafic volcanic rocks and slates are affected by chloritic alteration whereas felsic rocks present mainly sericitic (mica) alteration. More detailed information about the geology of the Riotinto deposits, including genetic and structural models can be found in Palomero (1990), Sáez et al. (1996, 1999), Tornos (2006), and Grande et al. (2010a).

2.2. The Marismillas reservoir and environmental framework

The Marismillas reservoir receives waters from one of the most emblematic rivers in the IPB — the Tinto River (Fig. 1). The river has its source in the mining area and, therefore, it is the main receptor of its drainage. It is a worldwide example of watercourse strongly affected by acid mine drainage processes. It has been intensively studied under distinctive perspectives (*e.g.*, Buckby et al., 2003; de la Torre et al., 2011; Grande et al., 2013a; Hubbard et al., 2009; Olías et al., 2006), including as an extreme ecological environment (Aguilera et al., 2007; Amils et al., 2007; Sánchez-Andrea et al., 2013). Besides the peculiar features of the Tinto River, the environmental impact caused by 5000 years of continuous mining is reflected in more than 1030 ha of affected landscape (Grande et al., 2013a). The dam, with a surface area of 70 ha, was built in 1878 to supply the mining complex. The reservoir receives waters with high content of soluble metals and sulphates mobilized by AMD processes in the river's headwaters. Furthermore, it has been subject to the input of particulate matter introduced both during seasonal rainfall and as a result of the failure of an ore washing dam located upstream. Consequently, the Marismillas reservoir is presently clogged with fine sediments and AMD-precipitates. In addition to mining contributions, Marismillas has a source of organic matter, due to the input of waste waters from the Nerva city. This impact of domestic waste water, which is poorly studied in AMD systems, deserves special attention since it may affect the behaviour of some elements present in the acidic reservoir.

3. Methods

3.1. Hydrochemical characterization

Water samples were collected every two weeks between October 2011 and May 2012, when the dry season arrived and water ceases to flow. Two sampling sites were selected, in order to represent the input water (L) and the water that exits the reservoir (C) (Fig. 1). During the hydrological year, a total of 15 samples were obtained.

The pH, temperature, electrical conductivity (EC), and total dissolved solids (TDS) were measured in the field with a multi-parameter meter (CRISON, MM). Before use, electrodes were calibrated and tested for accuracy, according to the manufacturer's instructions. Two samples were taken for laboratory analyses using polyethylene bottles (100 mL): one for sulphate and the other for metals. The sample for metals was filtered with 0.45 μm pore-diameter cellulose membrane filters and acidified with HNO_3 65% *suprapur* to prevent precipitation. After collection, samples were immediately refrigerated, kept in the dark and stored at 4 °C until analysis.

Sulphate was measured by photometry whereas metals and metalloids (Fe, Cu, Zn, Mn, Cd, Ni, Co, AS, Sb, Pb, and Al) were determined using atomic absorption air–acetylene spectroscopy (AAS), with a Perkin Elmer AAnalyst 800 (Perkin-Elmer, Norwalk), equipped with graphite furnace and hydride generator. The accuracy of the method was verified with certified reference samples. The measurement precision was greater than 5% RSD, whereas the detection limit was 0.1 μg/L for Cd, As, and Al and 1 μg/L for the rest of the elements.

3.2. Sediment sampling and analyses

The samples were collected in three drill cores (S1–S3), from the surface to the bottom of the reservoir, during the dry season (July 2011). The location of the drill cores was selected on the basis of a previous campaign, which allowed detecting geophysical anomalies (Fernandez et al., 2013). S1 and S2 (Fig. 1) were located in sites that have revealed positive magnetic and radar anomalies, respectively. In turn, S3 represents a negative magnetic anomaly. Sub-samples for geochemical and mineralogical analyses were obtained each 10 cm, given rise to 31 samples for S1, 38 for S2, and 37 for S3.

In order to obtain reference conditions for sediment chemistry, sampling and analyses were also performed in a clean reservoir located in the same regional, lithological, and metallogenic context (La Joya reservoir). Due to its location in an affluent without relevant mining influence, the water quality of La Joya reservoir is compatible with industrial use (Grande et al., 2013b). Therefore, this reservoir was used to represent the baseline conditions for the IPB.

3.2.1. Mineralogy

Mineralogical studies were carried out in two grain size fractions: <2 mm and <2 μm. The mineralogy of samples was analysed by X-ray powder diffraction (XRD) with a Philips X'pert Pro-MPD diffractometer (Philips PW 1710, APD), using Cu-Kα radiation. The XRD diffractograms were obtained from powders (bulk sample < 2 mm) and from oriented aggregates (<2 μm fraction) in the interval 3 to 65°2θ and 3 to 35°2θ, respectively. The equipment was operated with a 2 theta step size of 0.02° and a counting time of 1.25 s. The data obtained were treated with X'pert Pro-MPD software. Preparation procedures and the appropriated XRD conditions for these kinds of samples, in particular dealing with very low crystallinity materials, are described in Valente and Leal Gomes (2009).

Prior to analysis, the samples were air-dried and sieved to <2 mm grain size and then crushed and ground manually using an agate mortar and pestle. For the separation of <2 μm fraction, organic matter was previously removed by treating samples with H_2O_2 *p.a.*, following the procedure described by Larqué and Weber (1978). This fraction was, then, obtained by the sedimentation method and the particle-size separation based on theoretical Stockes' Law (Larqué and Weber, 1978; Moore and Reynolds, 1997). The clay mineralogy was determined using the oriented preparations, which were submitted to the following treatments: air-dried, ethylene glycol (EG)-solvated, and heated (490 °C).

Quantification of the <2 mm fraction was performed by using the peak-height intensities of the diagnostic reflections (Valente et al., 2012a, b). Estimation of clay minerals was deduced from the diagnostic peaks related to their first-order basal reflections at air-dried conditions or after EG solvation.

3.2.2. Sediment chemistry

Chemical contents of major and trace elements (Al, Fe, K, Na, Ca, Mg, S, P, As, Cu, Mn, Pb, Zn, Cr, Co, Ni, Se, Cd, and Sc) were obtained by inductively coupled plasma-mass spectrometry (ICP/MS) after an extraction with HF + $HClO_3$ + HNO_3 + HCl. These analyses were performed at laboratories of the R&D Central Services of the University of Huelva, including analysis of duplicate samples and blanks to check precision, whereas accuracy was obtained by using certified standards (SPEX series).

Table 1
Hydrochemical properties.

	L (input river waters) n = 15					C (output waters) n = 15				
	Average	Median	SD	Min	Max	Average	Median	SD	Min	Max
pH	2.19	2.22	0.13	1.92	2.42	2.21	2.19	0.17	1.92	2.67
T (°C)	17.94	17.60	4.42	12.80	31.20	18.99	18.00	4.99	12.60	31.20
EC (μs/cm)	9353	9940	1831	4750	11,000	11,249	11,950	2056	4750	13,190
TDS (mg/L)	5986	6360	1174	3040	7040	7214	7650	1323	3040	8430
SO_4^{2-} (mg/L)	2457	2400	698.6	1536	3960	2023	2032	714.7	996.0	3232
Fe (mg/L)	1435	1286	724.9	314.2	2954	1566	1352	675.4	321.5	3117
Cu (mg/L)	234.7	238.6	154.2	8.600	622.7	343.0	310.2	215.4	60.80	874.7
Zn (mg/L)	92.31	91.50	72.55	4.614	197.8	99.8	83.84	92.17	5.193	254.6
Mn (mg/L)	39.91	44.96	23.29	4.037	78.38	54.83	64.77	27.91	6.670	86.40
Cd (mg/L)	0.872	0.575	0.985	0.084	4.288	1.332	1.030	1.516	0.271	7.070
Ni (mg/L)	1.067	1.096	0.507	0.277	1.980	1.409	1.390	0.665	0.327	2.499
Co (mg/L)	8.661	8.136	6.262	2.579	26.68	9.883	8.826	5.778	2.591	27.86
As (mg/L)	2.100	1.688	2.116	0.000	7.911	2.510	1.465	3.404	0.000	14.10
Sb (mg/L)	0.124	0.037	0.242	0.004	0.965	0.078	0.041	0.082	0.000	0.268
Pb (mg/L)	0.635	0.482	0.456	0.125	2.009	0.682	0.618	0.436	0.153	2.083

4. Results

4.1. Hydrochemistry of Marismillas dam

The properties of the water are summarized in Table 1. They are typical acid sulphate waters, with an average pH around 2.2 and sulphate concentrations higher than 2000 mg/L (average values). Both sites, in the input and output waters, present high metal load with iron as the most abundant element, followed by Cu and Zn. Elements known by its toxicity, such as Co, As, Cd and Ni also occur in high concentrations. In particular, Co and As may reach contents up to 28 mg/L and 14 mg/L (maximum values), respectively.

Fig. 2 represents the average values obtained for trace elements in both sampling sites. In general, concentrations reach higher values in the output waters. The average pH (Table 1) is similar in both sites. Nevertheless, the pH range differs, showing higher fluctuation in the output waters.

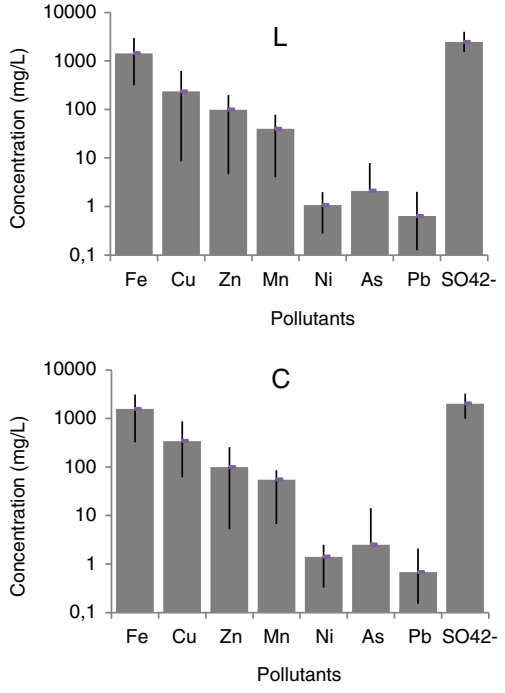

Fig. 2. Hydrochemistry of input (L) and output waters (C). Black bars on columns are standard error (n = 15).

Seasonal behaviour is represented in Fig. 3 through the representation of trace elements at the beginning of dry (May) and wet seasons (November). The analysed elements behave similarly in the two sites. For most of them, the highest contents were obtained in May. Zn and Mn are exceptions to this trend.

4.2. Mineralogical composition

The semi-quantitative mineralogical composition estimated by XRD in the <2 mm fraction is presented in Table 2 for the three drill cores. The detrital materials are composed by quartz, K-feldspar, plagioclase and mica. In the three cases, sulphides are represented by pyrite, pyrrhotite and marcasite. Also, the three reveal the presence of opala-CT, barite, siderite, and hematite. These minerals, with the exception of hematite, appear always in vestigial amounts (<5%). Another characteristic common to the three cores is the presence of typical AMD ochreous precipitates, namely goethite and jarosite. In general, the most abundant minerals in the <2 mm fraction are quartz, jarosite, mica, pyrrhotite, and hematite. Besides, clay minerals occur in low amounts (<5%). Mineralogy is very similar in the three drill cores; however there are some minor differences. For example, S2 is the only drill core with identifiable calcite and ankerite; magnesite and maghemite are absent in S1, whereas sulphur occurs only in S3.

Soluble salts, formed by evaporation of pore waters, were also identified. They are represented by the iron sulphates melanterite (in S1 and S2) and rozenite (S1, S2, and S3) and by the calcium sulphate anhydrite (S2).

In the clay sized fraction (Fig. 4), the mineralogical composition of tree drill cores is composed, in general, by clay minerals as chlorite, smectite and kaolinite. Also, associated minerals are present, such as goethite, jarosite, hematite and rhodochrosite.

The most abundant minerals in this fraction, in average, are illite, jarosite and kaolinite. Hematite, rhodochrosite and goethite are present in smaller amounts. The other clay minerals, namely chlorite and smectite occur in vestigial quantities. There are no significant differences in the composition of clay fraction of the three cores.

Fig. 5 presents XRD patterns of a sample, showing the typical d-reflexions of the identified minerals, including in the clay-size fraction. Jarosite was identified by the most important reflections at ~3.08 Å and ~3.11 Å, together with the series of reflections given by Brindley and Brown (1980). Generally, the XRD patterns show symmetric and sharp reflections (Fig. 5) indicating the presence of jarosite with high degree of order. On the contrary, goethite appears with diffraction broad and weak peaks at 4.16–4.18 Å and 2.69–2.70 Å. The large shape of the peaks and their low intensity seem to indicate the presence of poorly crystallized goethite.

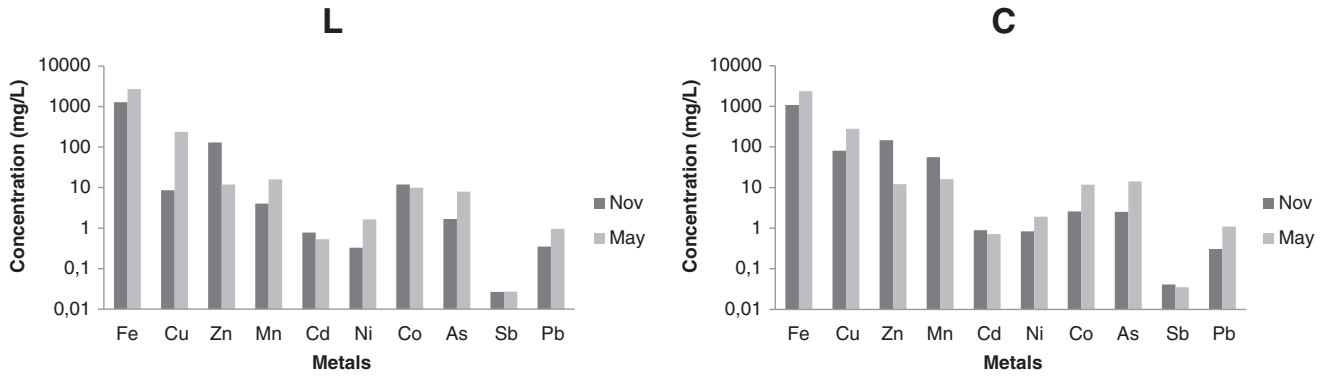

Fig. 3. Temporal variations of Marismillas waters.

Fig. 6 shows the relation between goethite, jarosite and pyrite in the sub-samples, with depth. The first two represent the typical ochreous AMD-precipitates, whereas pyrite was selected as the main primary precursor. Goethite is considerably less abundant than jarosite at all depths. Also, its contents are relatively stable in values <5%. On the contrary, jarosite varies considerably in the three cores in the range 5–25%. The spatial evolution in the three drill cores is identical, although there is some lag between them. For example, S1 is especially abundant in jarosite between 1 and 1.5 m depths, while S2 has a higher content around 2 m. In turn, in S3, the highest levels of jarosite are observed close to 2.5 m depth.

4.3. Chemical composition

Table 3 summarizes the chemistry of the material accumulated in the reservoir (fraction < 2 mm). The three cores show high contents of metals and metalloids (Cu, Zn, Pb, and As), which present average concentrations above 1000 mg/kg. Contamination by Pb and As is especially noted, with both elements reaching maximum concentrations of about 12,000 mg/kg in S2.

Fe and Al are major chemical components, although the average contents are near the baseline values obtained for La Joya sediments. However, most of the metals and metalloids, especially the ones of major environmental concern (As, Pb, Cu, Zn, Cd, and Co) are several orders of magnitude above the baseline values. Identical behaviour was observed for S, always above baseline. Also, P occurs with higher values, especially in S1. On the contrary, the sediments are impoverished in alkaline elements, such as Ca, Na, and Mg, as well as in Mn. In turn, similar contents of Cr occur in Marismillas and in the baseline reservoir. The majority of trace elements seem to present a short range of variability between the three drill cores. Nevertheless, S1 presents somewhat higher levels of Pb, As, and Ni.

Table 2
Estimation of the mineral composition by XRD of the <2 mm fraction.

Mineral (%)	S1	S2	S3
Quartz	Abundant	Abundant	Abundant
Opala-CT	Traces	Traces	Traces
Feldspar	Present	Present	Present
Plagioclase	Present	Present	Present
Mica	Present	Present	Present
Clay minerals	Traces	Present	Present
Jarosite	Present	Present	Present
Barite	Traces	Present	Present
Anhydrite	nd	Traces	nd
Melanterite	Present	Traces	nd
Rozenite	Traces	Traces	Traces
Magnesite	nd	Present	Traces
Rhodochrosite	Traces	Traces	Present
Siderite	Traces	Present	Traces
Calcite	nd	Traces	nd
Ankerite	nd	Traces	nd
Magnetite	Present	Traces	nd
Maghamite	nd	Traces	Traces
Hematite	Present	Present	Present
Goethite	Traces	Traces	Traces
Pyrite	Present	Present	Present
Pyrrhotite	Traces	Traces	Traces
Marcasite	Traces	Present	Present
Sulphur	nd	nd	Traces

<5% — traces; 5–25% — present; 27–75% — abundant; nd — not detected.

The association between major and trace elements was investigated by using the universe of samples. Fig. 7 shows the relationships between some abundant and relevant elements (Fe, Al, As, Cd, and Zn). Fe and Al show positive strong correlation, with Pearson coefficients of 0.999. Identically, As shows a very strong positive trend with both Fe and Al, with Pearson coefficients >0.73.

5. Discussion

Marismillas reservoir suffers the influence of AMD processes. This is demonstrated by values obtained for input and output waters, in agreement with results obtained by other authors (de la Torre et al., 2011) for the Riotinto area.

Comparing the two sampling sites (Fig. 1), L shows lower values of trace elements than site C (Fig. 2). This slight increase of pollutant concentration in water after being stored in the reservoir should be reflecting the input of mine wastes. At such low pH (<2.2, Table 1) dissolution occurs, including of the more inert minerals, such as silicates. The fine grain size of the accumulated material enhances the weathering processes. Therefore, output waters behave like a leachate carrying the mobilized elements. In addition, evaporation may be contributing for such higher concentrations in the outflowing waters.

Depending on pH and water chemistry fluctuations, trace elements undergo continual changes between dissolved, precipitated, and sorbed forms, as recorded in similar environments (Burt et al., 2011). Therefore, there is also retention of pollutants in the reservoir, namely through precipitation of supergenic minerals (*e.g.*, soluble salts and ochreous precipitates). This is demonstrated by slight decrease in sulphate observed in the output waters. Additionally, surface reactions on high specific surface phases, should play scavenge roles in the reservoir. These assumptions are suggested by the mineralogy and chemical composition of the accumulated material, as synthetized in Table 4. Data on pore water chemistry and saturation indexes, presently under evaluation, would allow validating the assumptions based on hydrochemistry and mineralogy.

5.1. Mineralogical hosts

The mineralogy of the reservoir indicates the presence of inherited minerals and of newly formed phases. The first type reflects the mineral assemblages of the ore paragenesis (*e.g.*, pyrite) and host rocks (*e.g.*,

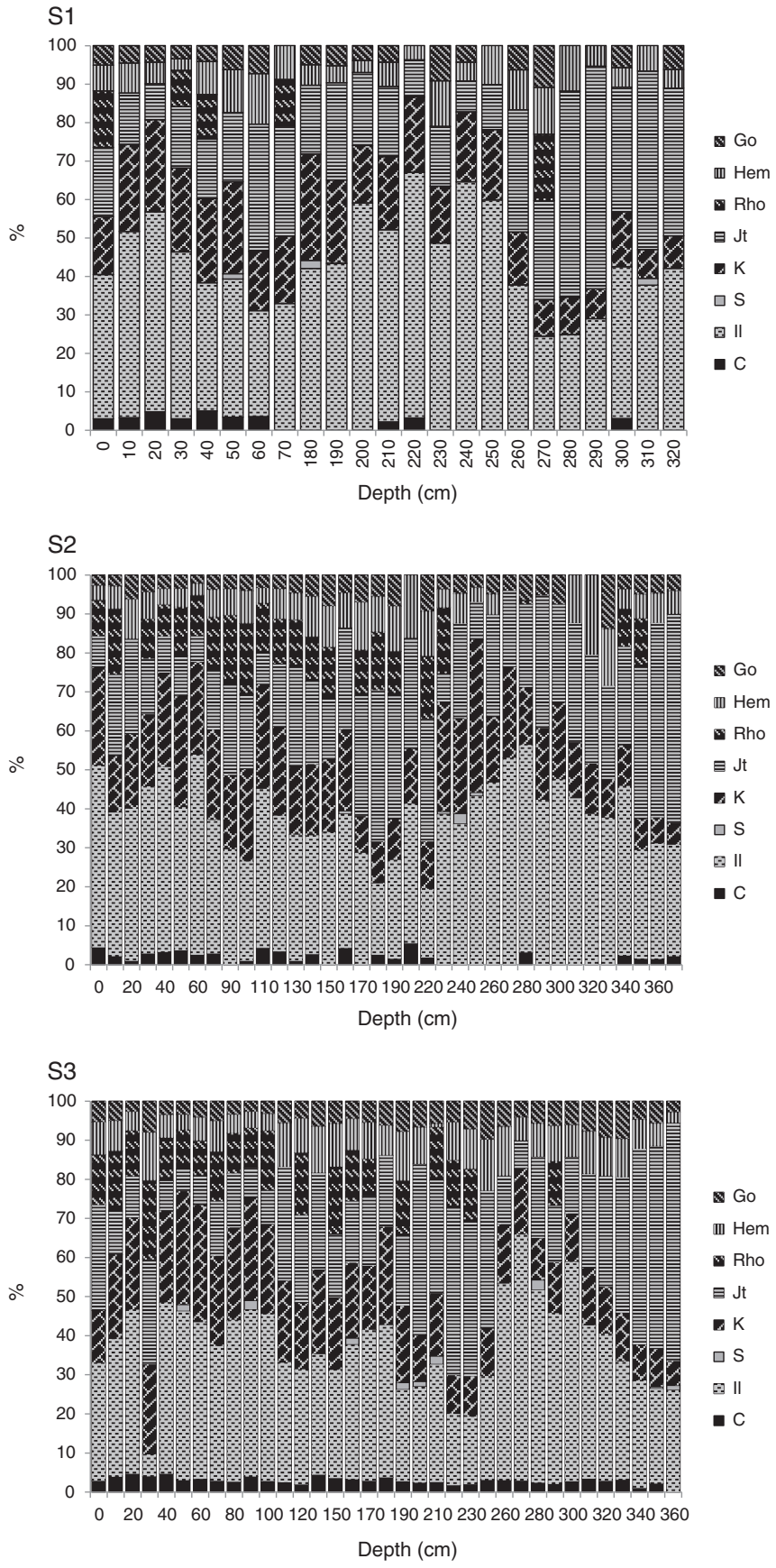

Fig. 4. Mineralogy of clay fraction.

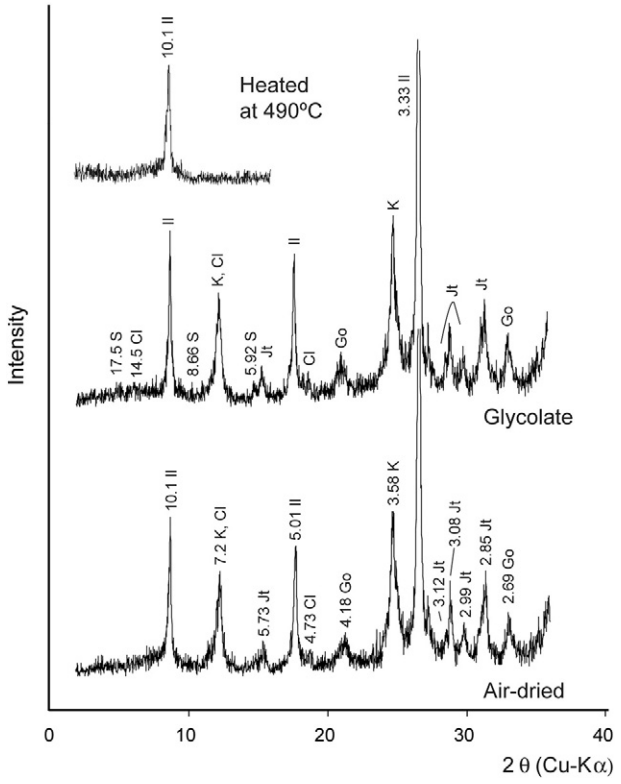

Fig. 5. XRD pattern of a typical sample.

mica and clay minerals, such as chlorite). They consist of particles that were dragged directly from waste dumps and ore piles. Among inherited minerals, there are also carbonates, such as rhodochrosite, siderite and ankerite. Their unexpected persistence in such strong acidic conditions may be due to passivation by iron precipitation. The second type of minerals, originated by chemical precipitation, comprises soluble salts and ochreous precipitates as summarized in Table 4. Both are known to play key roles in retention of metals in AMD environments (Jambor et al., 2000; Maia et al., 2012; Nordstrom and Alpers, 1999; Valente et al., 2013). However, their efficacy should be very dependent on seasonal fluctuations.

In the case of the hydrated sulphates (melanterite, rozenite and anhydrite, Table 4), their skill as sinks of Fe and other trace elements (Cu, Zn, and As) by precipitation, coprecipitation and adsorption (Jambor et al., 2000; Lottermoser, 2003; Nordstrom and Alpers, 1999) is controlled by solubility. Since their formation is driven by evaporation that allows reaching oversaturation, the retention of metals will be effective only in dry periods.

Regarding ochreous precipitates, the relationships between jarosite, goethite, and pyrite (Fig. 6) indicate that jarosite is always more abundant than goethite. These ochreous may be formed by direct oxidation of pyrite or by transformation controlled by pH and sulphate contents as stated in the literature (Bigham and Nordstrom, 2000; Bigham et al., 1994). Equilibrium conditions known for the relationship between jarosite and goethite (Acero et al., 2006; Bigham et al., 1994; Nordstrom and Alpers, 1999; Stoffregen et al., 2000) suggest that jarosite is stable in this pH range (pH < 2.2).

The vertical profiles of mineral distribution are different from others obtained in mining pit lakes and dams in other regions, where goethite

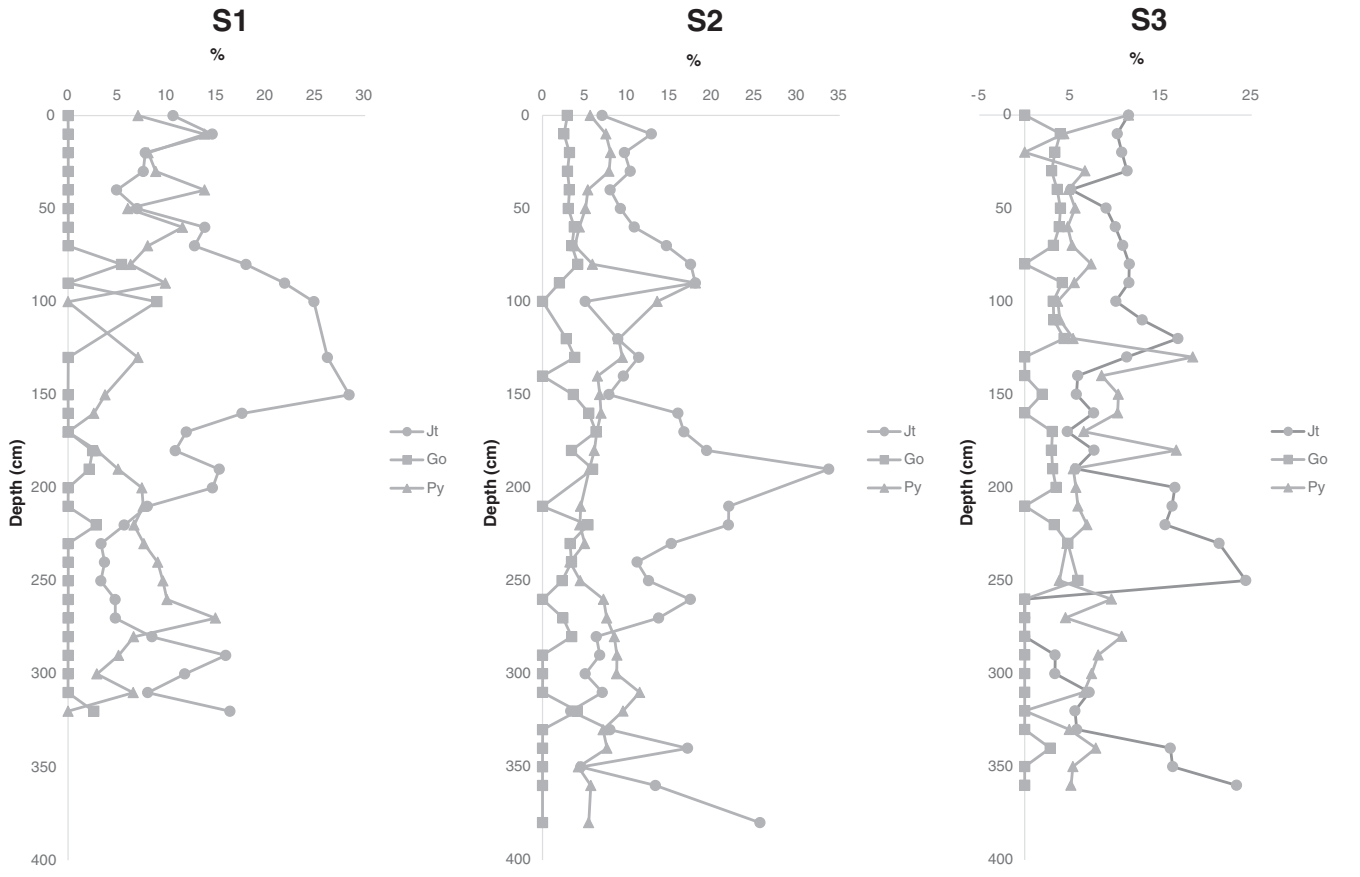

Fig. 6. Depth evolution of pyrite, jarosite and goethite in the three cores.

Table 3
Major and trace element composition analysed in the fraction <2 mm.

		%				mg/kg																		
		Al	Fe	K	S	As	Ba	Ca	Cu	Mg	Mn	Na	P	Pb	Ti	Zn	Cr	Co	Ni	Se	Cd	Sc
S1	Average	11.7	12.1	1.96	4.16	2952.5	2715.1	3090.1	1323.7	3224.9	174.50	2391.9	985.27	5180.1	3458.9	1027.3	77.043	24.956	61.206	19.216	5.6009	13.062
(n = 31)	Median	8.31	8.47	2.03	3.64	2275.1	2892.1	327.43	1115.1	3104.9	142.93	2265.0	1009.4	4977.9	3363.5	707.72	65.646	18.610	50.955	17.767	1.8370	12.854
	SD	7.68	8.20	0.74	1.87	1994.1	1048.3	15,130	841.11	1332.9	129.58	901.37	341.22	2250.4	1316.2	1201.4	43.325	20.031	46.554	8.8884	8.2113	5.0574
	Min	5.21	5.30	0.02	1.81	976.15	41.559	149.50	90.522	1207.1	52.238	521.26	422.06	61.311	51.381	190.15	15.602	74.652	2.3630	0.9296	0.4940	2.9638
	Max	31.0	33.1	3.23	10.2	9874.9	4491.7	84,605	3746.9	8170.9	722.57	4933.2	1900.9	10,038	5716.6	6616.8	192.56	106.55	219.98	49.085	35.008	25.382
S2	Average	9.43	9.69	1.97	3.42	2654.5	2270.3	372.69	1244.3	2941.2	145.84	2210.2	761.8	5528.8	3683.8	1174.8	60.777	19.501	18.913	16.123	3.5797	11.600
(n = 38)	Median	7.82	8.04	1.98	3.33	2338.4	2361.8	353.08	1090.9	2870.2	121.37	2197.8	730.58	5455.6	3738.3	656.26	59.501	13.463	14.94	14.607	2.2947	11.183
	SD	4.94	5.28	0.53	1.31	1898.3	7,39.69	128.71	814.10	695.35	70.998	389.45	191.48	1895.1	955.29	1566.6	25.086	20.316	13.910	6.2215	3.2554	2.7119
	Min	5.51	5.58	0.40	1.56	1156.3	584.63	138.59	246.00	1649.4	59.313	947.10	335.86	1595.2	627.84	200.82	30.937	57.209	4.8764	5.0824	0.4848	6.2254
	Max	29.6	31.9	3.35	7.64	12,109	3900.0	688.60	4369.1	4706.6	410.68	2887.3	1069.6	11,922	5325.5	8749.9	145.04	112.48	63.780	32.714	13.827	17.800
S3	Average	9.30	9.53	1.86	3.40	1983.3	2786.8	331.79	1479.9	2794.9	143.41	2227.5	714.68	4789.9	3551.9	974.46	66.191	24.883	23.901	14.661	5.3875	11.465
(n = 37)	Median	8.28	8.40	1.86	3.14	1734.5	2965.3	298.47	1055.5	2754.0	127.34	2174.3	613.77	5028.8	3517.3	511.69	67.736	14.528	18.375	13.469	2.2360	12.109
	SD	4.83	5.20	0.53	1.52	1262.8	924.60	127.33	1411.2	623.67	67.395	462.97	580.73	1672.1	1038.3	1017.1	24.683	33.737	22.036	5.0573	7.9817	28.399
	Min	5.39	5.48	0.13	1.74	1000.5	100.70	203.37	63.147	1696.1	77.591	454.42	229.79	161.59	295.33	192.24	33.779	67.329	10.316	2.8683	0.2796	3.8543
	Max	32.5	35.0	2.58	9.18	8344.6	3984.6	710.56	7447.3	4890.0	449.80	2917.4	3533.5	9469.3	5054.9	5142.8	160.4	207.67	108.88	25.724	43.405	15.807
La Joya		8.60	3.88	1.76	0.02	12.071	303.54	6111.8	25.479	5898.8	614.20	5261.6	237.64	22.088	4190.7	60.593	69.579	15.269	–	1.7328	0.1787	20.154

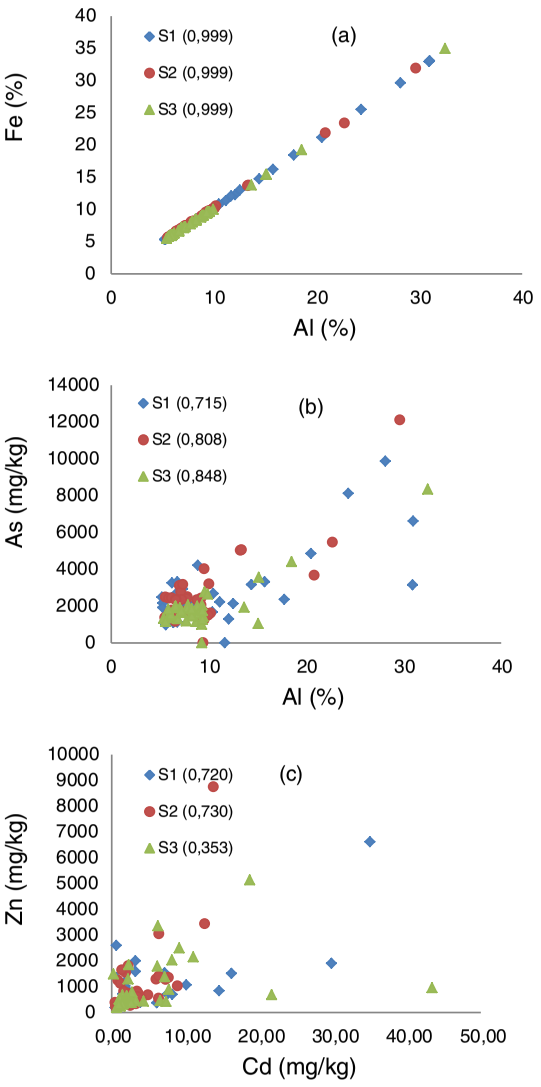

Fig. 7. Relationships between elements in the clogging material. Pearson coefficients are provided in the graphs. (a) Al *vs* Fe; (b) Al *vs* As; (c) Cd *vs* Zn.

tends to replace jarosite (and schwertmannite) with time. Therefore, the dominance of jarosite could be a proxy of the sediment age. Transformation to goethite may be retarded or even precluded either by very high sulphate concentrations and/or a very low pH. So, the small amounts of goethite relative to jarosite (Fig. 6) may be justified by the higher stability of the second in such acidic conditions (Eq. (1)). In this case, the low pH is acting as a strong chemical inhibitor for the formation of goethite. However, after strong rainy periods, some dilution and, consequently, neutralization are expected, allowing transformation to goethite. The low crystallinity of goethite, suggested by the broad reflexions in XRD patterns (Fig. 5), confirms the instability of goethite relative to jarosite.

$$KFe_3(SO_4)_2(OH)_{6(s)} \leftrightarrow 3\,FeO(OH)_s + K^+_{(aq)} + 2SO_4{}^{2-}{}_{(aq)} + 3H^+_{(aq)} \quad (1)$$

In addition to the minerals identified by XRD, amorphous precipitates made of iron and sulphate are expected to form under these conditions, in agreement with results obtained by Valente et al. (2012b). Further research on this reservoir should be focused on nanoprecipitates (defined as <100 nm in size). Their morphology, chemistry and stability should play a key role in controlling the fate

Table 4
Summary of the composition of the accumulated material. Q = quartz; O-CT = opala-CT; F = K-feldspar; P = plagioclase; Mi = mica; CM = clay minerals; Jt = jarosite; Ba = barite; Anh = anhydrite; Mel = melanterite; Roz = rozenite; Mg = magnesite; Rho = rhodochrosite; Sid = siderite; Ank = ankerite; Mgn = magnetite; Mgh = maghemite; Hem = hematite; Go = goethite; Py = pyrite; Pyr = pyrrhotite; Marc = marcasite; Su = sulphur.

Composition		<2 mm fraction		
		S1	S2	S3
Inherited minerals		Q > Mi > Py > P = Hem > F = CM > Marc = Rho = Sid > Pyr > Ba = Mg = Mgn = Mgh = O-CT	Q > Mi > Hem = Py > P > F = CM > Marc = Rho = Sid > Pyr = Ba > Ca = Mg = Ank = Mgn = Mgh = O-CT	Q > Mi > Py > P = Hem > F = CM = Sid > Marc > Rho > Ba = Pyr = Su > Mg = Mgn = Mgh = O-CT
Supergene minerals	Ochre-precipitates	Jt ≫ Go	Jt ≫ Go	Jt ≫ Go
	Soluble salts	Mel > Roz	Anh = Roz	Roz
Geochemistry		Fe ≈ Al > Pb > As > Cu > Zn > Mn	Fe ≈ Al > Pb > As > Cu > Zn > Mn	Fe ≈ Al > Pb > Ba > As > Cu > Zn > Mn

and environmental relevance of the trace elements in the Marismillas reservoir.

5.2. Geochemical trends

Fig. 6 shows linear relationships between Fe, Al, and As, suggesting a close association in the sediments. In general, correlations can be explained by the source of input of the elements or by their geochemical behaviour, namely mobility or retention in specific mineralogical hosts. So, the behaviour of Fe and Al (Fig. 7a) indicates strong positive correlation ($r^2 = 0.999$) between major elements mobilized from the source materials, both sulphides (Fe) and felsic host rocks (Al). Also, Cd and Zn are typical of sphalerite composition. So, their close relation in S1 and S2 ($r^2 \approx 0.73$, Fig. 7) can be due to the common primary source, although this sulphide has not been identified by XRD analyses. Furthermore, As appears highly correlated with Al ($r^2 = 0.74$–0.88) and with Fe ($r^2 = 0.73$–0.88). These associations may indicate that As is being retained by iron-rich materials, such as jarosite, as described by other authors (Iskandar et al., 2012). In fact, jarosite is a member of the isostructural jarosite–alunite group of minerals, with As and Al being often included in its structure (Hudson-Edward and Edwards, 2005), which could be contributing to such correlation. The obtained associations also suggest that Al-phases, like the clay minerals may be retaining As. However arsenic aqueous species are anionic or neutral at low pH, which difficult their adsorption onto clay minerals. This is an interesting issue to develop on the Marismillas sediments. Sequential extraction and spectroscopic techniques, namely X-ray absorption fine structure, are being prepared to apply to the sediments as they could provide evidence that As is being retained by the clay minerals, mainly smectite.

5.3. Enrichment factors

The geochemistry of the sediments (Table 3) exposes the influence of mining contamination through the high contents of elements with typical mining source, such as sulphur and trace elements. However there are also signs of organic contamination. This indication is provided by the high content of P, relative to the baseline conditions. In the absence of phosphate minerals from the host rocks, its presence must be due to the income of domestic waste water. Moreover, the highest content was observed in the drill core closest to the source of waste water.

Often, enrichment factors (EFs) are determined relative to geochemical background, which represents the natural element concentration, for example using pre-anthropogenic sediments, such as in the work by Borrego et al. (2013). In the present study, the concept of baseline conditions as defined by Salminen and Gregorauskiene (1997) was preferred to obtain enrichment factors. Here, baseline obtained in La Joya reservoir represents reference concentrations in a region under human disturbance, such as the case of IPB, allowing monitoring environmental changes, as stated by Yanguo et al. (2002).

The EF reflects the degree of enrichment of an element by dividing its ratio to a normalizing element by the ratio found in the baseline (Borrego et al., 2013; Covelli an Fontolan, 1997; Lee et al., 1997; Prudêncio et al., 2010; Yanguo et al., 2002). This calculus performs in accordance with Eq. (2), where El is the concentration of the potentially enriched element and Sc is the concentration of the proxy element. In the present work, normalization was carried out by using Sc, as its geochemical behaviour is similar to that of Al, but it has weaker activity in the supergene environment (Yang et al., 2010). EF > 1 denotes that the trace element acts like a pollutant.

$$EF = [(El)/(Sc)]_{Marismillas}/[(El)/(Sc)]_{baseline} \quad (2)$$

Fig. 8 plots the enrichment factors for metals and metalloids in the Marismillas reservoir. EF follows the order As ≈ Pb > Cu > Cd > Zn > Se > Fe > Co > Al, providing indication about strong contamination,

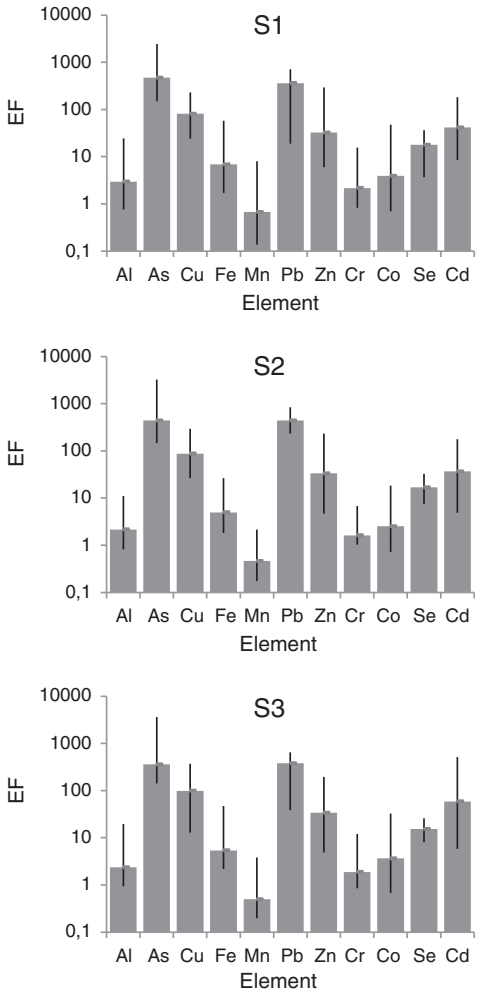

Fig. 8. Enrichment factors. Black bars on columns are standard error (n = 31–38).

particularly by Pb and As. On the contrary, Mn shows EF < 1, which confirms this metal poverty relative to the baseline concentrations. In the cases of As and Pb, EFs are in the range from 358–471. In agreement with classification proposed by Sutherland (2000), such values indicate extreme pollution by As, Pb, Cu, and Cd since EF > 40. Such enrichment processes should be related with the concentration of trace elements in clay minerals and in the ochreous precipitates, jarosite and goethite. Furthermore, since the sampling campaign was carried out in summer, under very dry conditions, coprecipitation and adsorption on rozenite and melanterite may also contribute to such enrichment as observed by Valente et al. (2013) for soluble salts formed in the Tharsis mines, also in the IPB.

6. Conclusions

Historic mining activities in the Riotinto area together with natural contamination by ARD have resulted in water and sediment contamination of Marismillas reservoir. Moreover, transport of particulate matter and chemical precipitation led to the clogging of the reservoir. Concentrations of trace elements in water showed variability among two sites: in the input river waters and in output waters, with higher values at the last site. This was explained by the contribution of mine wastes dragged from waste dumps and by geochemical and mineralogical evolution undergone in the reservoir. Mineralogy of the clogged material showed a short-range of spatial variability since XRD analyses indicated similar composition for the three drill cores. Among the newly formed phases, jarosite and goethite are the most abundant. Combining data about mineral distribution and crystallinity, suggests that jarosite forms directly from sulphide oxidation, whereas goethite my result from transformations undergone in the reservoir.

The geochemistry of the clogging material revealed high contents of elements mobilized from AMD/ARD processes. Analysis of geochemical trends indicated that Fe, Al and As are strongly correlated in the sediments. This association suggests that As is being retained by iron-rich materials, such as jarosite and, probably, by Al-phases like the clay minerals identified in the reservoir.

The extent of the enrichment in trace elements in Marismillas was assessed relative to a clean reservoir used to define baseline conditions for the IPB (La Joya reservoir). The results demonstrated that Marismillas sediments are strongly enriched in environmental and economic relevant trace elements. Higher EFs were obtained for As and Pb (358–471), followed by Cu (EF near 100).

Acknowledgements

Financial support for this research was provided by DGCICYT National Plan, project CGL2010-21268-C02-01. CIG-R is supported by the national budget of the Portuguese Republic through FCT — under the project PEst-OE/CTE/UI0697/2011. The authors thank to António Azevedo for his help in XRD analysis and to Elisabete Vivas for her assistance with the preparation of clay fraction. Also, the authors are grateful to Dr Irwan Iskandar and to an anonymous reviewer for their valuable contributions for the manuscript.

References

Acero, P., Ayora, C., Torrentó, C., Nieto, J.M., 2006. The behaviour of trace elements during schwertmannite precipitation and subsequent transformation into goethite and jarosite. Geochim. Cosmochim. Acta 70, 4130–4139.

Adamides, N., 2013. Rio Tinto (Iberian Pyrite Belt): a world-class mineral field reopens. Appl. Earth Sci. 122, 2–15.

Aguilera, A., Souza-Egipsy, V., Gómez, F., Amils, R., 2007. Development and structure of eukaryotic biofilms in an extreme acidic environment, Río Tinto SW, Spain. Microb. Ecol. 53, 294–305.

Amils, R., González-Toril, E., Fernández-Remolar, D., Gómez, F., Agillera, A., Rodríguez, N., Malki, M., García-Moyano, A., Fairén, A., de la Fuente, V., Sanz, J., 2007. Extreme environments as Mars terrestrial analogues: the Rio Tinto case. Planet. Space Sci. 55, 370–381.

Bigham, J.M., Nordstrom, D.K., 2000. Iron and aluminum hydroxysulfates from acid sulfate waters. In: Alpers, C.N., Jambor, J.L., Nordstrom, D.K. (Eds.), Sulfate Minerals: Crystallography, Geochemistry and Environmental Significance. Rev. Mineral Geochem 40, pp. 351–403.

Bigham, J.M., Carlson, L., Murad, E., 1994. Schwertmannite, a new iron oxyhydroxysulphate from Pyhasalmi, Finland, and other localities. Mineral. Mag. 58, 641–648.

Borba, R.P., Figueiredo, B.R., 2003. Geochemical distribution of arsenic in waters, sediments and weathered gold mineralized rocks from Iron Quadrangle, Brazil. Environ. Geol. 44, 39–52.

Borrego, J., Carro, B., Grande, J.A., de la Torre, M.L., Valente, T., Santisteban, M., 2013. Control factors on the composition of superficial sediments in estuaries of the coast of Huelva (SW Spain): a statistical approach. J. Iber. Geol. 39, 223–239.

Brindley, G.W., Brown, G., 1980. Quantitative X-ray Mineral Analysis of Clays: in Crystal Structures of Clay Minerals and Their X-ray Identification, Monograph No. 5. Mineralogical Society, London, pp. 411–438.

Buckby, T., Black, S., Coleman, M.L., Hodson, M.E., 2003. Fe-sulfate-rich evaporative mineral precipitates from the Rio Tinto, southwest Spain. Mineral. Mag. 67, 263–278.

Burt, R., Weber, T., Park, S., Yochum, S., Ferguson, R., 2011. Trace element concentration and speciation in selected mining-contaminated soils and water in Willow Creek Floodplain, Colorado. Appl. Environ. Soil Sci. 2011.

Cáceres, L., Olías, M., Andrés, J., Rodríguez-Vidal, J., Clemente, L., Galván, L., Medina, B., 2013. Geochemistry of Quaternary sediments in terraces of the Tinto River (SW Spain): paleoenvironmental implications. Catena 101, 1–10.

Cánovas, C.R., Hubbard, C.G., Olías, M., Nieto, J.M., Black, S., Coleman, M.L., 2008. Hydrochemical variations and contaminant load in the Río Tinto (Spain) during flood events. J. Hydrol. 350, 25–40.

Carro, B., Borrego, J., López-González, N., Grande, J.A., Gómez, T., de la Torre, M.L., Valente, T., 2011. Impact of Acid Mine Drainage on the hydrogeochemical characteristics of the Tinto–Odiel Estuary (SW Spain). J. Iber. Geol. 37, 87–96.

Carvalho, J., Sousa, P., Matos, J.X., Pinto, C., 2011. Ore prospecting in the Iberian Pyrite Belt using seismic and potential-field data. J. Geophys. Eng. 8, 1–12.

Cheng, H., Hu, Y., Xu, B., Zhao, J., 2009. Geochemical processes controlling fate and transport of arsenic in acid mine drainage (AMD) and natural systems. J. Hazard. Mater. 15, 13–26.

Covelli, S., Fontolan, 1997. Application of a normalization procedure in determining regional geochemical baselines. Environ. Geol. 30, 34–45.

Davis, R.A., Welty, A.T., Borrego, J., Morales, J.A., Pendon, J.G., Ryan, J.G., 2000. Rio Tinto estuary (Spain): 5000 years of pollution. Environ. Geol. 39 (10), 1107–1116.

de la Torre, M.L., Grande, J.A., Jiménez, A., Borrego, J., Díaz Curiel, J., 2009. Time evolution of an AMD affected river chemical makeup. Water Resour. Manag. 23, 1275–1289.

de la Torre, M.L., Grande, J.A., Graiño, J., Gómez, T., Ceron, J.C., 2011. Characterization of AMD pollution in the river Tinto (SW Spain). Geochemical comparison between generating source and receiving environment. Water Air Soil Pollut. 216, 3–19. http://dx.doi.org/10.1007/s11270-010-0510-1.

de Oliveira, D.P.S., Matos, J.X., Rosa, C.J.P., Rosa, D.R.N., Figueiredo, M.O., Silva, T.P., Guimarães, F., Carvalho, J.R.S., Pinto, A.M.M., Relvas, J.R.M.S., Reiser, F.K.M., 2015. The Lagoa Salgada orebody, Iberian Pyrite Belt, Portugal: geology, distribution, mineralogy and geochemistry of Indium. Economic GeologySEG, Colorado USA (in press, 23 pp.).

Elbaz-Poulichet, F., Braungard, C., Achterberg, E., Morley, N., Cossa, D., Beckers, J., Nomérange, P., Cruzado, A., Leblanc, M., 2001. Biogeochemistry in the Tinto–Odiel rivers (Southern Spain) and in the Gulf of Cadiz: a synthesis of the results of TOROS project. Cont. Shelf Res. 21, 1961–1973.

Evangelou, V.P., Zhang, Y.L., 1995. A review: pyrite oxidation mechanisms and acid mine drainage prevention. Crit. Rev. Environ. Sci. Technol. 25, 141–199.

Fernandez, J.P., Borrego, J., Viñuela, I., Grande, J.A., de la Torre, M.L., Valente, T., Santisteban, M., 2013. Contribution of GPR and magnetic methods to the definition of the internal structure of a clogged mining dam in the Rio Tinto mine, South West Spain. Water Resources Forest, Oc. & Marine ecosystem, pp. 735–743. http://dx.doi.org/10.5596/sgem2013.

Fernández-Caliani, J.C., Barba-Brioso, C., González, I., Galán, E., 2009. Heavy metal pollution in soils around the abandoned mine sites of the Iberian Pyrite Belt (Southwest Spain). Water Air Soil Pollut. 200, 211–226.

Fernández-Remolar, D.C., Gómez-Elvira, J., Gómez, F., Sebastián, E., Martín, J., Manfredi, J.A., 2004. The Tinto river, an extreme acidic environment under control iron, as an analog of the Terra Meridiani hematite site of Mars. Planet. Space Sci. 52, 239–248.

Galán, E., Gómez-Ariza, I., GTonzález, J.C., Fernández-Caliani, Morales, E., Giráldez, I., 2003. Heavy metal partitioning in river sediments severely polluted by acid mine drainage in the Iberian Pyrite Belt. Appl. Geochem. 18, 409–421.

Grande, J., 2011. Impact of AMD processes on the public water supply: hydrochemical variations and application of a classification model to a river in the Iberian Pyritic Belt S.W. Spain. Hydrol. Res. 42, 472–478.

Grande, J.A., de la Torre, M.L., Cerón, J.C., Beltrán, R., Gómez, T., 2010. Overall hydrochemical characterization of the Iberian Pyrite Belt. Main acid mine drainage-generating sources (Huelva, SW Spain). J. Hydrol. 390, 123–130.

Grande, J.A., Aroba, J., Andújar, J., Gómez, T., de la Torre, M.L., Borrego, J., Romero, S., Barranco, C., Santisteban, M., 2011. Tinto versus Odiel: two AMD polluted rivers and an unresolved issue. An artificial intelligence approach. Water Resour. Manag. 25 (14), 3575–3594.

Grande, J.A., Valente, T., de la Torre, M.L., Santisteban, M., Cerón, J.C., Perez-Ostale, E., 2013a. Characterization of acid mine drainage sources in the Iberian Pyrite Belt: base methodology for quantifying affected areas and for environmental management. Environ. Earth Sci. http://dx.doi.org/10.1007/s12665-013-2652-0.

Grande, J.A., Santisteban, M., de la Torre, M.L., Valente, T., Pérez-Ostalé, E., 2013b. Characterisation of AMD pollution in the reservoirs of the Iberian Pyrite Belt. Mine Water Environ. http://dx.doi.org/10.1007/s10230-013-0236-6.

Gray, N.F., 1996. Field assessment of acid mine drainage contamination in surface and ground water. Environ. Geol. 27, 358–361.
Hubbard, C., Black, S., Coleman, M., 2009. Aqueous geochemistry and oxygen isotope composition of acid mine drainage from the Rio Tinto, SW Spain, highlight inconsistencies in current models. Chem. Geol. 265, 321–334.
Hudson-Edwards, K.A., Edwards, S.J., 2005. Mineralogical controls on storage of As, Cu, Pb and Zn at the abandoned Mathiatis massive sulphide mine, Cyprus. Mineral. Mag. 69, 695–706.
Iskandar, I., Koike, K., Sendjaja, P., 2012. Identifying groundwater arsenic contamination mechanisms in relation to arsenic concentrations in water and host rocks. Environ. Earth Sci. 65, 2015–2026.
Jambor, J.L., Nordstrom, D.K., Alpers, C.N., 2000. Metal-sulfate salts from sulfide mineral oxidation. In: Alpers, C.N., Jambor, J.L., Nordstrom, D.K. (Eds.), Sulfate Minerals: Crystallography, Geochemistry, and Environmental Significance. Mineralogical Society of America, Washington, DC, pp. 305–350.
Keith, C.N., Vaughan, D.J., 2000. Mechanisms and rates of sulphide oxidation in relation to the problems of acid rock (mine) drainage. In: Campbell, L.S., Valsami-Jones, E., Batchelder, M. (Eds.), Environmental Mineralogy: Microbial Interactions, Anthropogenic Influences, Contaminated Land and Waste. The Mineralogical Society Series 9, pp. 117–139.
Larqué, P., Weber, F., 1978. Techniques de preparation des minéraux argileux en vue de l'analyse par diffraction des rayons-X. Notes techniques de l'Institut de Géologie. Université Louis Pasteur de Strasbourg (33 pp.).
Lee, P., Touray, J., Ballif, P., 1997. Trace metal contamination of settling particles in a retention pond along the A-71 motorway in Sologne, France. Sci. Total Environ. 201, 1–15.
López-Archilla, A., Gérard, E., Moreira, D., López-García, P., 2004. Macrofilamentous microbial communities in the metal-rich and acidic River Tinto, Spain. FEMS Microbiol. Lett. 235, 221–228.
Lottermoser, B., 2003. Mine Wastes — Characterization, Treatment and Environmental Impacts. Springer, Berlin (277 pp.).
Maia, F., Pinto, C., Waerenborgh, J., Gonçalves, M., Prazeres, C., Carreira, O., Sério, S., 2012. Metal partitioning in sediments and mineralogical controls on the acid mine drainage in Ribeira da Água Forte (Aljustrel, Iberian Pyrite Belt, Southern Portugal). Appl. Geochem. 27, 1063–1080.
McKibben, A.A., Barnes, H.L., 1986. Oxidation of pyrite in low temperature acidic solutions: rate laws and surface textures. Geochim. Cosmochim. Acta 50, 1509–1520.
Moore, D.M., Reynolds, J.R.C., 1997. X-ray Diffraction and the Identification and Analysis of Clay Minerals. Oxford University Press, New York (378 pp.).
Nieto, J., Sarmineto, A., Olias, M., Avora, C., 2013. Acid mine drainage in the Iberian Pyrite Belt: 1. Hydrochemical characteristics and pollutant load of the Tinto and Odiel rivers. Environ. Sci. Pollut. Res. 20, 7509–7519.
Nordstrom, D.K., Alpers, C.N., 1999. Negative pH, efflorescent mineralogy, and consequences for environmental restoration at the Iron Mountain Superfund site, California. Proc. Natl. Acad. Sci. U. S. A. 96, 3455–3462.
Nordstrom, D.K., Southam, G., 1997. Geomicrobiology of sulfide mineral oxidation. In: Benfield, J.F., Nealson, K.H. (Eds.), Geomicrobiology: Interactions Between Microbes and Minerals. Reviews in Mineralogy 35. Mineralogical Society of America, pp. 361–390.
Olias, M., Canovas, C.R., Nieto, J.M., Sarmiento, A.M., 2006. Evaluation of the dissolved contaminant load transported by the Tinto and Odiel rivers (South West Spain). Appl. Geochem. 21, 1733–1749.
Palomero, F.G., 1990. Rio Tinto deposits — geology and geological models for their exploration and ore-reserve evaluation. In: Gray, P.M.J., et al. (Eds.), Sulphide Deposits—Their Origin and Processing. The Institution of Mining and Metallurgy, pp. 17–35.
Prudêncio, M.I., Dias, M.I., Ruiz, F., Waerenborgh, J.C., Duplay, J., Marques, R., Franco, D., Ben Ahmed, R., Gouveia, M.A., Abad, M., 2010. Soils in the semi-arid area of the El Melah Lagoon (NE Tunisia) — variability associated with a closing evolution. Catena 80, 9–22.
Ruiz, F., Borrego, J., González-Regalado, M.L., López, N., Carro, B., Abad, M., 2008. Impact of millennial mining activities on sediments and microfauna on the Tinto River estuary (SW Spain). Mar. Pollut. Bull. 56, 1258–1264.
Sáez, R., Almodóvar, G.R., Pascual, E., 1996. Geological constraints on massive sulphide genesis in the Iberian Pyrite Belt. Ore Geol. Rev. 11, 428–451.
Sáez, R., Pasqual, E., Toscano, M., Almodovar, G.R., 1999. The Iberian type of volcano-sedimentary massive sulphide deposits. Mineral. Deposita 34, 549–570.
Salminen, R., Gregorauskiene, V., 1997. Considerations regarding the definition of geochemical baseline of elements in the surficial materials in areas differing in basic geology. Appl. Geochem. 15, 647–653.
Sánchez-Andrea, I., Stams, A., Amils, R., Sanz, J., 2013. Enrichment and isolation of acidophilic sulfate-reducing bacteria from Tinto River sediments. Environ. Microbiol. Rep. 5, 672–678.
Sánchez-España, J., López Pamo, E., Santofimia, E., Aduvire, O., Reves, J., Barettino, D., 2005. Acid mine drainage in the Iberian Pyrite Belt (Odiel river watershed, Huelva, SW Spain): geochemistry, mineralogy and environmental implications. Appl. Geochem. 20, 1320–1356.
Sánchez-Rodas, D., Gómez-Ariza, J.L., Giraldez, I., Velasco, A., Morales, E., 2005. Arsenic speciation in river and estuarine waters from southwest Spain. Sci. Total Environ. 345 (1–3), 207–217.
Sarmiento, A.M., Nieto, J.M., Casiot, C., Elbaz-Poulichet, F., Egal, M., 2009. Inorganic arsenic speciation at river basin scales: the Tinto and Odiel Rivers in the Iberian Pyrite Belt, SW Spain. Environ. Pollut. 157, 1202–1209.
Sobron, P., Rull, F., Sobron, F., Sanz, A., Medina, J., Nielsen, C.J., 2007. Raman spectroscopy of the system iron(III)–sulfuric acid–water: an approach to Tinto River's (Spain) hydrogeochemistry. Spectrochim. Acta A 68, 1138–1142.
Stoffregen, R.E., Alpers, C.N., Jambor, J.L., 2000. Alunite–jarosite crystallography, thermodynamics and geochronology. In: Alpers, C.N., Jambor, J.L., Nordstrom, D.K. (Eds.), Sulfate Minerals: Crystallography, Geochemistry, and Environmental Significance. Mineralogical Society of America, Washington, DC, pp. 453–479.
Stoker, C.R., Cannon, H.N., Duganan, S.E., Lemke, L.G., Glass, B.J., Miller, D., 2008. The 2005 MARTE robotic drilling experiment in Río Tinto, Spain: objectives, approach, and results of a simulated mission to search for life in the Martian subsurface. Astrobiology 8, 921–945.
Sutherland, R., 2000. Bed sediment-associated trace metals in an urban stream, Oahu, Hawaii. Environ. Geol. 39, 611–627.
Tornos, F., 2006. Environment of formation and styles of volcanogenic massive sulfides: the Iberian Pyrite Belt. Ore Geol. Rev. 28, 259–307.
Valente, T., Leal Gomes, C., 2009. Occurrence, properties and pollution potential of environmental minerals in acid mine drainage. Sci. Total Environ. 407, 1135–1152.
Valente, T., Gomes, P., Pamplona, J., de la Torre, M.L., 2012a. Natural stabilization of mine waste-dumps — evolution of the vegetation cover in distinctive geochemical and mineralogical environments. J. Geochem. Explor. 123, 152–161.
Valente, T., Antunes, M., Sequeira Braga, A., Prudêncio, I., Marques, R., Pamplona, J., 2012b. Mineralogical attenuation for metallic remediation in a passive system for mine water treatment. Environ. Earth Sci. 66, 39–54.
Valente, T., Grande, J.A., de la Torre, M.L., Santisteban, M., Cerón, J.C., 2013. Mineralogy and environmental relevance of AMD-precipitates from the Tharsis mines, Iberian Pyrite Belt (SW, Spain). Appl. Geochem. 39, 11–25.
Vicente-Martorell, J.J., Galindo-Riaño, M.D., García-Vargas, M., 2009. Bioavailability of heavy metals monitoring water, sediments and fish species from a polluted estuary. J. Hazard. Mater. 162, 823–836.
Yang, Y., Li, S., Bi, X., Wu, P., Liu, T., Li, F., Liu, C., 2010. Lead, Zn, and Cd in slags, stream sediments, and soils in an abandoned Zn smelting region, southwest of China, and Pb and S isotopes as source tracers. J. Soils Sediments 10, 1527–1539.
Yanguo, T., Shijun, N., Xianguo, T., Chengjiang, Z., Yuxiao, M., 2002. Geochemical baseline and trace metal pollution of soil in Panzhihua mining area. Chin. J. Geochem. 21, 274–281.